ILASS–Europe 2022, 31th Conference on Liquid Atomization and Spray Systems, 6-8 September 2022, Virtual, Israell

Pressure Swirl Spray Characteristics Under Cross-flow

Ondrej Cejpek*[1], Milan Maly[1], Ondrej Hajek[1], Frantisek Prinz[1], Madan Mohan Avulapati[2], Jan Jedelsky[1]

[1] Energy Institute, Brno University of Technology, Brno, Czech

[2]Indian Institute of Technology Tirupati, Renigunta Road, Tirupati – 517 506, India

*Corresponding author: Ondrej.Cejpek@vutbr.cz

Abstract

The pressure swirl atomizers (PSAs) are used in a wide range of agriculture and combustion applications where ambient flow applies. The PSAs form a hollow cone-type spray, with high concentration of droplets at spray periphery, where droplets appear in a wide size range (1 – 100 μm). The spray quality (e.g. droplet size) is governed by the liquid sheet thickness at its breakup position. The sheet thickness reduces with the breakup length increase and thus the spray quality is expected to improve. A smooth and undistorted liquid sheet breaks up at a large distance from the nozzle under still ambient air conditions. The liquid sheet formation under the cross-flow condition differs from that in still conditions. The flowing air increases the relative sheet-air velocity with two consequences: 1) it reduces the primary breakup length as the disrupting forces on the sheet increase, and 2) it promotes the secondary liquid breakup and intensifies the spray mixing so the droplet size reduces. The present study aims to investigate the spill-return pressure swirl spray with optical diagnostic tools such as PDA and high-speed visualization. The effects of 1) the inlet pressure (P_{in} = 0.25, 0.5 and 1 MPa), 2) the Spill-to-feed ratio, *SFR* (defined as a ratio of the flow rate through the spill-line to the flow rate through the inlet ports and 3) the cross–flowing air (0 – 35 m/s) on the spray were investigated.

Keywords

Conical liquid sheet, subsonic cross-flow, pressure swirl atomizer, Laser Doppler diagnostics

Introduction

The spill return pressure swirl atomizer (PSSA) can be used in a variety of applications, e.g. in combustion, agriculture, flue gas cleaning, and many more. The main advantage is its simple design, robust behavior and good turndown ration. Most of works focused on the investigation of PSSA under still laboratory conditions, and relationship between operating conditions and the resulting spray characteristics was investigated. The main focus was devoted to spray cone angle (*SCA*), breakup length (l_b), and droplet characteristics such as Sauter mean diameter (*SMD*) and Integral Sauter mean diameter (*ISMD*). The extensive research was done by Maly et al. [1] [2] [3] in recent years.

The PSSA are deployed in a variety of applications, and ambient conditions differ widely. Atomizers work in high-temperature high-speed flows in combustion processes, raised temperatures with swirling flows are present in flue gas cleaning, flows with different scaled vortices are found in the agriculture. Only a few papers investigated sprays under realistic ambient flow conditions. Lynch et al. [4] investigated the pressure swirl atomizer (PSA) under combustion conditions (air heated to 533 K with flow in the range from 7 to 30 m/s with turbulent intensities (Tu) approximately 6%. Prakash et al. [5] focused on the primary breakup of liquid sheet under cross-flowing air in range from 8 to 90 m/s. Leeward and windward spray side breakup differently. Zhang et al. [6] investigated droplet dispersion in cross-flow deploying PIV method. Lee et al. [7] investigated breakup length and penetration height of PSA in low speed cross-flow. Breakup length was derived for the leeward and windward side separately. Leeward side exhibit shorter breakup length. The breakup length determination is not

described and measurement uncertainties are not provided. No study was found to investigate the influence of cross-flow on spray cone angle (*SCA*), Integral Sauter mean diameter (*ISMD*) *and* breakup length (l_b) of PSSAs

This study tries to expand the knowledge provided in [1] [2] [3] to cross-flow conditions and investigates the influence of cross-flowing air on *SCA*, *lb,* and *ISMD*. Correlations for spray characteristics are provided. The authors believe that this knowledge can improve the atomizer design for different applications, where ambient flow applies.

2 Experimental setup

The experimental setup used for the investigation of pressure swirl spray in cross-flow is described in the following sections. The wind tunnel, fuel circuit, Phase Doppler anemometry and high-speed visualization setups are covered in detail.

2.1 Wind tunnel facility

The small-scale, low-speed wind tunnel was specially designed for the spray experiment in realistic conditions. The wind tunnel is arranged in a blow-down arrangement. The test section dimensions are 200 × 200 × 400 mm, flow velocity can be set from 8 to 40 m/s with Tu < 1%.

2.2 Fuel circuit and tested atomizer

Water was used as testing liquid. The supply system is illustrated in Figure 1 left. Water from a storage tank (1) is supplied to a pressure swirl atomizer (6). The gear pump (3) is used in series with a filter (2). The mass flow rate is measured using a Coriolis mass flow meter (4) (Mass 2100 Di3 containing Mass 6000 transmitter, Siemens AG, GE) with an accuracy of ±0.1% from the actual flow rate. Inlet and spill-line pressure were measured with piezo-resistive BD Sensor DMP 33li (BD SENSORS s.r.o., CZ) (5) and (6) respectively. Pressure was measured with an accuracy of ±2 kPa. The amount of liquid flowing in the spill-line was controlled with a valve (9) and the mass flow of the liquid was measured using the flow meter DOM-S05 (KOBOLD Messring GmbH, GE) (8). The accuracy of the flow meter is ±1% of actual flow rate. The schematic layout of investigated PSSA atomizer is illustrated in Figure 1 right. Water is supplied into the swirl chamber through the tangential ports. The liquid acquires the swirl motion in the swirl chamber and is discharged through the exit orifice. The liquid forms a conical liquid sheet that subsequently disintegrates into ligaments and droplets. The dimensions of spill-line arrangement are illustrated in the Figure 1 right. The spill-line arrangement in Figure 1 right was used in [2].

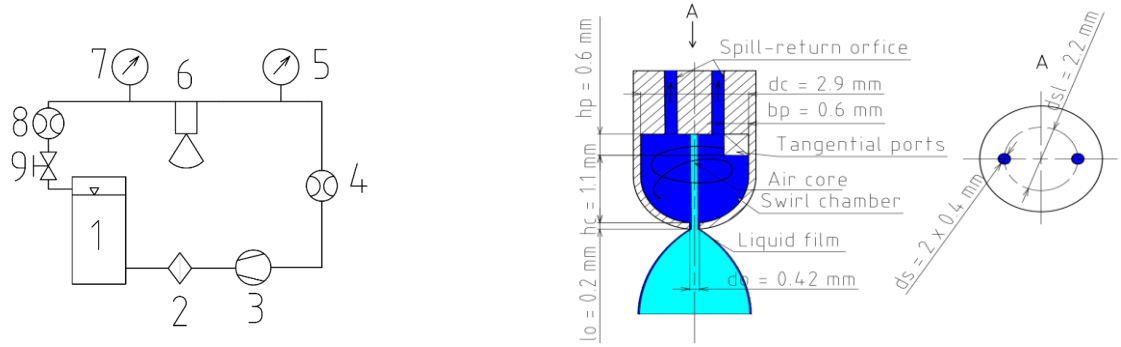

Figure 1.: Fuel circuit (left), PSSA (right)

2.3 *PDA measurement setup*

Droplets size and velocity were determined using a two-component fibre-based PDA measurement system (Dantec Dynamics A/S Skovlunde, DK). The schematic layout of the measurement setup is illustrated in Figure 2 left. The setup is described in Figure 2 right.

Measurement was carried out in coincidence mode. Two-component velocity along with the simultaneous drop sizes were acquired. Two planes were probed at different axial positions Z = 10 mm, and 20 mm defined from the nozzle tip. In each plane, 2 perpendicular axes were measured. At each point either 50,000 samples were acquired, or a 10-second acquisition duration was achieved. The Dantec BSA 5.2 software was used to control the measurement.

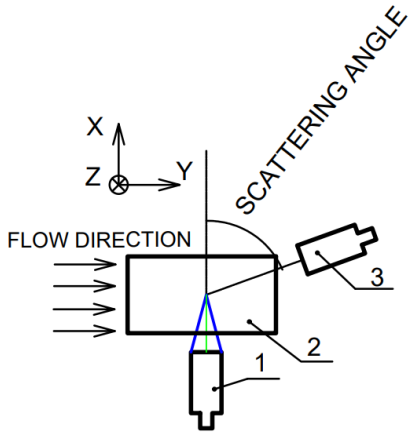

1 TRANSMITTING OPTICS 60X81
2 TEST SECTION
3 RECEIVING OPTICS 57X50

Parameter	Value	
Laser power output	0.35 W	
Scattering angle	48 °	
Receiver mask	B	
Receiver spatial filter	0.1 mm	
Focal length of transmitting/receiving optics	500/500 mm	
Wavelength	488 nm	514.5 nm
Velocity component	Axial	Radial
Velocity centre	19 m/s	0 m/s
Velocity span	51 m/s	73 m/s
Sensitivity	800 V	1050 V
SNR	0 dB	0 dB
Signal gain	8 dB	10 dB
Level validation ratio	8	2

Figure 2.: PDA setup (left), PDA parameters (right)

2.4 *High-speed visualization*

A high-speed camera FASTCAM SA-Z type 2100K-M-16GB (Japan) was used to capture an instantaneous image of a spray under cross-flow conditions. The LED light model HPL3-36DD18B (Lightspeed Technologies) was used to illuminate the spray. The *SCA* was derived from a set of 2000 images separately for each liquid film side. In-house code in MATLAB was used. The high-speed images were divided into two parts, each containing only one liquid film side. Edge detection was applied to find the boundaries of the liquid film. The liquid film boundaries were then fitted with a robust fit with linear function and *SCA* was determined by line slope for each liquid side separately. The standard mean deviation of the *SCA* was ± 2°. The l_b of each liquid film side was also determined by in-house Matlab code. 2000 images were analyzed, resulting in a standard deviation of l_b ±1.5 mm. The SCA and l_b are illustrated in Figure 3.

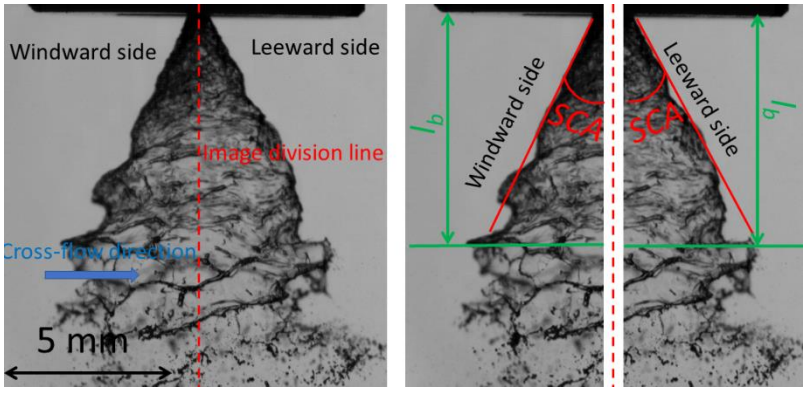

Figure 3.: *SCA* and l_b of liquid sheet in cross-flow

3 Results and discussion

The results obtained by the experiments were analyzed and are outlined in the following sections. The effect of cross-flow on the is discussed followed by spray characteristics such as *SCA*, l_b, and *ISMD*.

3.2 Effect of cross-flow on the SCA

The spray cone angle is very important spray characteristics. It determines the aerodynamic interactions with surrounding flows, the area covered with a spray, and the relative velocity of droplets and air direction. The *SCA* for the leeward and windward side is illustrated in Figure 4 left for different liquid-to-air momentum ratios (*q*). The q can be computed by following equation $q = \rho_l v_l^2 / \rho_a v_a^2$, where ρ_l, ρ_a and v_l, v_a are densities of liquid and air and velocities of liquid and air, respectively. The *SCA* is the same for the leeward and windward side for $q \geq 2000$, due to the high liquid momentum. The *SCA* differs for windward and leeward liquid side for low *q*. The liquid sheet bends in the direction of cross-flow, which causes smaller windward *SCA* and a larger leeward *SCA*. The largest difference between windward and leeward *SCA* were observed for the breakup regimes of the collapsing sheet, double bag, and single bag (described in [5]).

Maly et al. [2] derived a PSSA equation for *SCA* operating under still conditions (equation 1) utilizing injection pressure (p_l) and *SFR*. Equation 1 is accurate (R^2 = 0.8) only for q = 2000, where *SCA* is not influenced by the ambient flow. For lower *q,* equation 1 underestimates the *SCA*. The *q* was implemented to equation 1 to account the cross-flow of air. The *SCA* (sum of leeward and windward *SCA*) in cross-flow can be predicted by equation 2. The correlation is outlined in Figure 4 right.

$$SCA = 16.3 p_l^{0.1} (1 - SFR)^{-0.15} \quad (1)$$

$$SCA = 60 p_l^{0.1} (1 - SFR)^{-0.15} q^{-0.2} \quad (2)$$

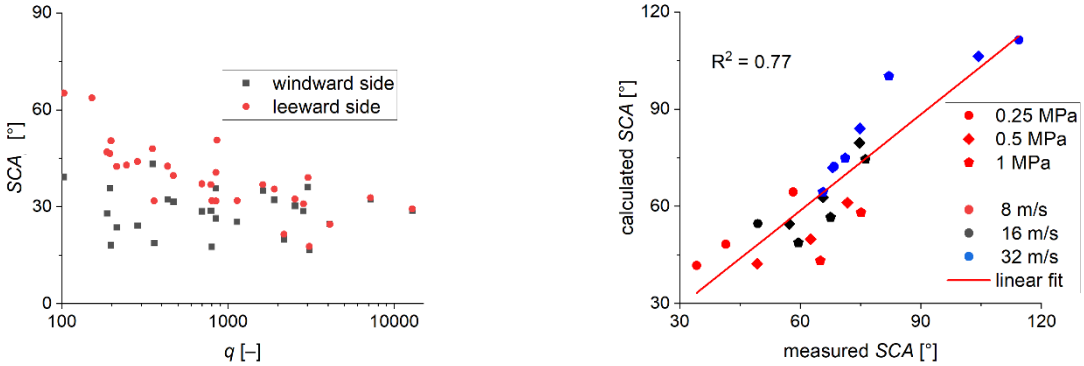

Figure 4.: *SCA* for the leeward and windward sides for different *q* (left), comparison of measured and computed SCA (right)

3.3 Effect of cross-flow on the breakup length

The l_b influences the droplet and the ligament diameter. The liquid film with a larger l_b creates smaller droplets and vice versa. The l_b is the same for the windward and leeward side (difference in l_b is smaller than the l_b repeatability). The l_b of the windward side is illustrated in Figure 5 left. There is a rapid decrease of l_b for small cross-flow Weber number (We_{cf}). $We_{cf} = \rho_a v_a^2 d_o / \sigma$.

Maly et al. [2] correlated l_b with p_l and m_{inj}. We extended this correlation for the cross-flow conditions (equation 3). Equation 3 utilizes only p_l and *q*. The m_{inj} is incorporated into *q*. The comparison of measured and calculated l_b is illustrated in Figure 5 right.

$$l_b = 32 p_l^{-0.8} q^{0.25} \quad (3)$$

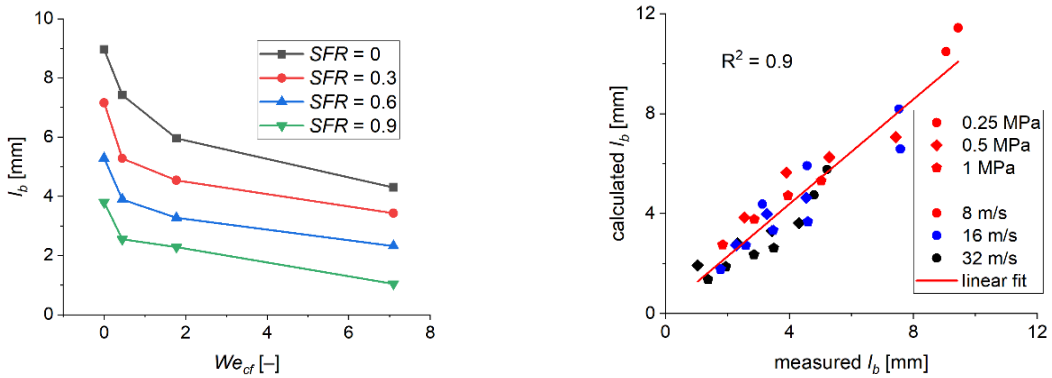

Figure 5.: l_b for different We_{cf} (left), comparison of measured and computed l_b (right)

3.4 Effect of cross-flow on ISMD

ISMD expresses the *SMD* representative for the whole spray. With increasing the cross-flow velocity *ISMD* also increases because small droplets are carried away by the cross-flow. The *ISMD* in *Z* = 20 mm is higher partially due to the droplet coalescence, but also by the cross-flow effect and even larger droplets are carried away by the cross-flow. The data for *SFR* = 0.9 must be taken with care due to a small number of droplets in measurement positions. Maly et al. [2] corelated *ISMD* with p_l, l_b and *SFR* with R^2 = 0.85. This correlation was extended with We_{cf} for cross-flow applications (equation 4). The ISMD $\propto We_{cf}^{0.11}$ is valid in *Z* = 10 mm, in *Z* = 20 mm the effect of We_{cf} is more prominent ($We_{cf}^{0.2}$). The *ISMD* is illustrated for different We_{cf}, *SFR*, and *Z* in Figure 6 left. The comparison of measured and computed *ISMD* is illustrated in Figure 6 right.

$$ISMD = 61.5 \cdot 10^{-4} p_l^{-0.33} l_b^{-0.18} (1 - SFR)^{0.1} We_{cf}^{0.11} \quad (4)$$

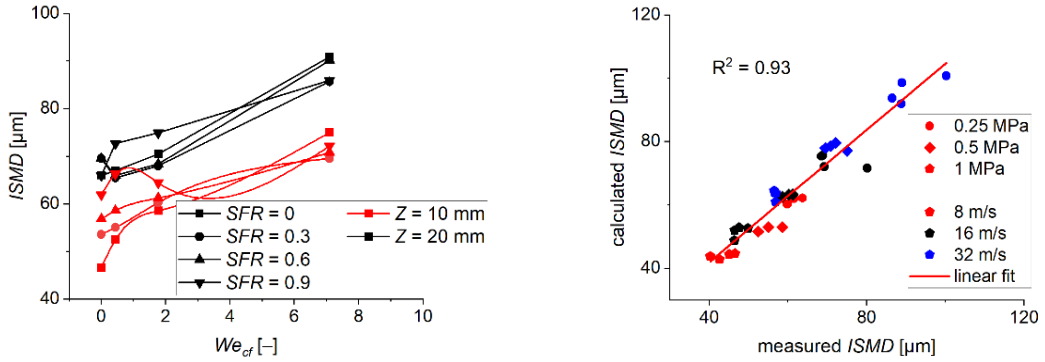

Figure 6.: *ISMD* for different We_{cf}, *SFR* and axial location from the nozzle (left), comparison of measured and computed *ISMD* (right)

4 Conclusions

The PSSA was investigated under cross-flow conditions in the velocity range from 8 to 32 m/s with *Tu* < 1%. High-speed visualization and PDA measurement were performed. The main emphasis was put on the spray characteristics (*SCA*, l_b, *ISMD*) under cross-flow conditions. The *SCA* of the windward and leeward side *was* determined. The *SCA* differs for low *q*, where cross-flow penetrates inside the spray cone. For *q* ≥ 2000 the *SCA* in cross-flow can be predicted by equation in [2]. The correlations for *SCA, lb, and ISMD* proposed in [2] were extended to cross-flow conditions. The windward and leeward sides exhibit the same l_b, which was correlated with p_l and *q* with R^2 = 0.89. *ISMD* was found to increase with $We_{cf}^{0.11}$ for *Z* = 10 mm and with $We_{cf}^{0.2}$ for *Z* = 20 mm. The *SCA* and l_b were correlated with *q*, *ISMD* with

We_{cf}. This implies that the behavior is influenced mainly by q near the nozzle, but far from the nozzle, where droplets are present, We_{cf} plays the major role.

Acknowledgments

The authors acknowledge the financial support from the project no. LTAIN19044 program INTER–EXCELLENCE (INTER–ACTION) by the Ministry of Education, Youth and Sports of the Czech Republic., project Quality Internal Grants of BUT (KInG BUT), Reg. No. CZ.02.2.69 / 0.0 / 0.0 / 19_073 / 0016948, which is financed from the OP RDE, the project “Computer Simulations for Effective Low-Emission Energy Engineering” funded as project No. CZ.02.1.01/0.0/0.0/16_026/0008392 by Operational Programme Research, Development and Education, Priority axis 1: Strengthening capacity for high-quality research. and from No. FSI-S-20-6295 founded by Fa;culty of Mechanical Engineering, Brno University of Technology.

References

[1] M. Maly *et al.*, "Internal flow and air core dynamics in Simplex and Spill-return pressure-swirl atomizers," *International Journal of Heat and Mass Transfer,* vol. 123, pp. 805-814, 2018/08/01/ 2018, doi: https://doi.org/10.1016/j.ijheatmasstransfer.2018.02.090.

[2] M. Maly, M. Sapik, O. Cejpek, G. Wigley, J. Katolicky, and J. Jedelsky, "Effect of spill orifice geometry on spray and control characteristics of spill-return pressure-swirl atomizers," *Experimental Thermal and Fluid Science,* vol. 106, pp. 159-170, 2019.

[3] M. Maly, O. Cejpek, M. Sapik, V. Ondracek, G. Wigley, and J. Jedelsky, "Internal flow dynamics of spill-return pressure-swirl atomizers," *Experimental Thermal and Fluid Science,* vol. 120, p. 110210, 2021/01/01/ 2021, doi: https://doi.org/10.1016/j.expthermflusci.2020.110210.

[4] A. Lynch, R. G. Batchelor, B. Kiel, J. Miller, J. Gord, and M. F. Reeder, "SPRAY CHARACTERISTICS OF A PRESSURE-SWIRL FUEL INJECTOR SUBJECTED TO A CROSSFLOW AND A COFLOW," vol. 21, no. 8, pp. 625-643, 2012-02-24 2011, doi: 10.1615/AtomizSpr.2012004012.

[5] R. Surya Prakash, H. Gadgil, and B. N. Raghunandan, "Breakup processes of pressure swirl spray in gaseous cross-flow," *International Journal of Multiphase Flow,* vol. 66, pp. 79-91, 2014/11/01/ 2014, doi: https://doi.org/10.1016/j.ijmultiphaseflow.2014.07.002.

[6] H. Zhang, B. Bai, L. Liu, H. Sun, and J. Yan, "Droplet dispersion characteristics of the hollow cone sprays in crossflow," *Experimental Thermal and Fluid Science,* vol. 45, pp. 25-33, 2013/02/01/ 2013, doi: https://doi.org/10.1016/j.expthermflusci.2012.09.021.

[7] S. Lee, W. Kim, and W. Yoon, "Spray formation by a swirl spray jet in low speed cross-flow," *Journal of Mechanical Science and Technology,* vol. 24, no. 2, pp. 559-568, 2010/02/01 2010, doi: 10.1007/s12206-009-1222-6.